# Methane detection with a near-infrared heterodyne phase-sensitive dispersion spectrometer at a stronger frequency modulation using direct injection-current dithering

Haojie Zhang, Tao Wu, Qiang Wu, Weidong Chen, Chenwen Ye, Mengyu Wang, Ming Zhu, Xingdao He

Research Article | Vol. 31, No. 15 / 17 Jul 2023 / Optics Express 25070
Optics EXPRESS

# Methane detection with a near-infrared heterodyne phase-sensitive dispersion spectrometer at a stronger frequency modulation using direct injection-current dithering

HAOJIE ZHANG,[1] TAO WU,[1,*] QIANG WU,[2] WEIDONG CHEN,[3] CHENWEN YE,[1] MENGYU WANG,[4] MING ZHU,[1] AND XINGDAO HE[1]

[1]*Key Laboratory of Nondestructive Test (Ministry of Education), Nanchang Hangkong University, Nanchang, 330063, China*
[2]*Department of Mathematics, Physics and Electrical Engineering, Northumbria University, Newcastle upon Tyne, NE1 8ST, UK*
[3]*Laboratoire de Physicochimie de l'Atmosphère,Université du Littoral Côte d'Opale 189A, Av. Maurice Schumann, 59140 Dunkerque, France*
[4]*Jiangxi Etcho Industry Co., Ltd., Nanchang, 330063, China*
[*]*wutccnu@nchu.edu.cn*

**Abstract:** Heterodyne phase-sensitive dispersion spectrometer (HPSDS) retrieves the concentration of gas samples by measuring the refractive index fluctuations near the molecular resonance. Compared to previous HPSDS studies focusing on pure intensity modulation, it is attractive to investigate the performance of HPSDS sensor based on a distributed feedback (DFB) laser under conditions where frequency modulation is much higher than intensity modulation. In this work, we report the implementation of a near-infrared HPSDS for methane detection based on the direct modulation of a DFB laser. The performance of our HPSDS is assessed using the characteristic absorption peak of methane near 1653.7 nm. Long-time measurements show that our HPSDS has a detection limit (MDL) of 1.22 ppm at standard atmospheric pressure and room temperature. In the same experimental conditions, we have experimentally compared HPSDS to wavelength modulation spectroscopy (WMS) to evaluate the dynamical range, long-term stability, and precision limits of the two methods.



## 1. Introduction

Methane ($CH_4$) is one of the most important greenhouse gases and exerts a strong impact on the global climate [1]. Methane is also a flammable and explosive gas, and real-time monitoring of $CH_4$ gas concentration plays a significant role in preventing accidental explosions. Overall, high-precision measurements of $CH_4$ concentration have a great relevance for applications. In particular, detectors able to measure concentration changes over a wide range are valuable for different scenarios, such as underground mines, combustion process diagnosis, and industrial process control.

Different techniques have been developed for gas sensing and $CH_4$ detection [2–5]. Among them, tunable diode laser absorption spectroscopy (TDLAS) is one of the most widely used techniques due to its non-contact nature, strong selectivity, high sensitivity, and fast response time [6,7]. TDLAS techniques include direct absorption spectroscopy (DAS) and wavelength modulation spectroscopy (WMS). DAS relies on the fact that when a laser resonates with a gas absorption line, the light intensity is weakened by absorption according to the Beer-Lambert law [8]. In DAS, a baseline fitting is required to properly take into account the laser power

#495581 https://doi.org/10.1364/OE.495581
Journal © 2023 Received 16 May 2023; revised 23 Jun 2023; accepted 24 Jun 2023; published 13 Jul 2023

Optics EXPRESS

transmission. However, this baseline is usually several orders of magnitude higher than the measured signal intensity. Moreover, factors such as thermal radiation, beam steering, and floating particles along the light path, usually cause power fluctuations [9], thereby limiting the sensitivity of the system. In WMS, the laser wavelength is modulated with a high frequency sine signal, and the harmonic signal, carrying the gas concentration information, is demodulated by a lock-in amplifier. In this way, there is no need for baseline fitting, and the 1/$f$ noise is suppressed by moving the signal to a higher frequency region, overall improving the measurement sensitivity [10]. However, WMS signals are still sensitive to laser power fluctuations, and this requires normalization of the received light power. Rieker et al. measured WMS-2f signals normalized by the first harmonic generation (2f/1f) to reduce the effects of optical power fluctuation, at least to some extent [11]. In both DAS and WMS, as the Beer-Lambert relationship is an exponential model, the absorption signal linearly depends on the gas concentration only for weak absorption, i.e. $\alpha(v) < 0.05$. For measurements involving strongly absorbing samples, the signal becomes insensitive to the variation of concentration, and needs to be corrected for its nonlinear dependence [12].

In dispersion spectroscopy, one studies the properties of a sample by measuring the fluctuations of the refractive index around the molecular resonance [13,14]. However, the change in refractive index is a process accompanied by gas absorption, which is inherent to molecular transitions. The dispersion of optical phase signals, which is related to the refractive index, can be related to the absorption coefficient through the Kramers-Kronig relations [15]. Therefore, gas concentration can be characterized by measuring the dispersion spectrum. Compared to TDLAS based on measuring light intensity attenuation, dispersion spectroscopy has a larger linear dynamic range, does not require a baseline, and is immune to laser power fluctuations [16,17]. Among the detection schemes based on the laser dispersion spectrum, chirped laser dispersion spectroscopy (CLaDS) proposed by Wysocki et al. represents an interesting method [18]. In CLaDS, one retrieves the dispersion spectrum by demodulating the instantaneous frequency shift of the beat note signal with a chirped frequency laser. This requires a high-performance real-time radio-frequency spectrum analyzer (usually very expensive) to measure the frequency fluctuations [19]. The output signal is proportional to the laser chirp rate, which puts additional requirements for the modulation rate of the laser and the laser controller [20]. Heterodyne phase sensitive dispersion spectroscopy (HPSDS) is a recently proposed dispersion spectrum detection method for monitoring gas concentration [21]. In HPSDS, a three-tone laser beam (double sideband signal) is generated by intensity modulation of a tunable laser, and then the optical phase shift between the sidebands is extracted by a lock-in amplifier [22]. HPSDS inherits the advantages of CLaDS but has a simpler structure and an easy signal processing, which makes it suitable for applications in the field of spectral gas sensing.

There are two different implementations of HPSDS: one is achieved by intensity modulation of the laser output through an external modulator; the other is achieved by directly modulating the injection current of the semiconductor lasers via a RF bias-tee circuit. So far near-infrared HPSDS gas sensing systems have been mostly developed using a DFB laser with an expensive intensity modulator to obtain a three-tone signal [23–25]. The three-tone optical beam can also be generated by directly modulating current of a laser, however, it inevitably introduces synchronous intensity modulation (IM) and frequency modulation (FM) [26,27]. This leads to asymmetry in amplitude and phase for the two sidebands, in turn, induces a nonlinear relation between the output phase and the gas concentration. Since quantum cascade lasers (QCLs) have a small linewidth enhancement factor, frequency modulation can be minimized at high frequencies (hundreds of MHz) by selecting the appropriate operating point of the laser, so FM is much smaller than IM. This unique modulation characteristic of QCL allows it widely used in mid-infrared HPSDS [28,29]. For the DFB laser, the FM is still much higher than the IM even at very high frequency (GHz) conditions [30,31]. It is interesting to study HPSDS sensor

Optics EXPRESS

performance at different operating points of DFB lasers under conditions where FM is much higher than IM. Following this idea, in this paper we report on the design and implementation of a near-infrared HPSDS sensor for methane detection using the characteristic absorption peak of $CH_4$ near 1653.7 nm. The sensor performance at different scanning frequencies, modulation frequencies and laser bias currents is studied. Moreover, in the same experimental conditions, we compare WMS and HPSDS to assess their dynamical range, long-term stability, and precision limits.

## 2. Experimental principle

HPSDS retrieves the gas concentration by measuring the variation of the refractive index near the molecular resonance. The refractive index is related to the absorption coefficient through the Kramers-Kronig relation [32]:

$$n(\omega) = 1 + \frac{c}{\pi}\int_0^{+\infty} \frac{\alpha(\omega')}{\omega'^2 - \omega^2} d\omega' \tag{1}$$

where $c$ is the speed of light in vacuum, $\omega$ is the frequency, and $\alpha(\omega)$ and $n(\omega)$ are the absorption coefficient and refractive index at $\omega$, respectively. A spectrum composed of a carrier wave ($E_0$) and two sidebands ($E_1$, $E_{-1}$), i.e a three-tone laser beam, is generated by directly modulating the injection current of a laser. But this modulation scheme will inevitably introduce both IM and FM simultaneously. In the vicinity of a molecular resonance, each tone senses a different change in refractive index. Therefore, when the beam passes through the gas sample, these three components are transmitted with different phase velocities, resulting in an optical phase shift [23]. The three tones can be expressed as [27]:

$$E_0 = e^{-\frac{\alpha(\omega_0)L}{2}} I\cos(\omega_0 t - \varphi_0) \tag{2}$$

$$E_1 = e^{-\frac{\alpha(\omega_0+\Omega)L}{2}} \frac{m}{4} I\left\{\cos[(\omega_0+\Omega)t - \varphi_1] + \frac{2\beta}{m}\cos[(\omega_0+\Omega)t - \theta - \varphi_1]\right\} \tag{3}$$

$$E_{-1} = e^{-\frac{\alpha(\omega_0-\Omega)L}{2}} \frac{m}{4} I\left\{\cos[(\omega_0-\Omega)t - \varphi_{-1}] - \frac{2\beta}{m}\cos[(\omega_0-\Omega)t + \theta - \varphi_{-1}]\right\} \tag{4}$$

where

$$\varphi_k = \frac{(\omega + k\Omega)L}{c}[n(\omega + k\Omega) - 1]. \tag{5}$$

The coefficient k = 0, 1, -1;where $\varphi_0$, $\varphi_1$ and $\varphi_{-1}$ are the phases of the carrier wave $E_0$ and the two sidebands $E_1$ and $E_{-1}$, respectively, $I$ is the laser intensity, $L$ is the absorption path length, $\omega_0$ is the central frequency, $\Omega$ is the modulation frequency, $m$ is the IM index (defined as the amplitude of IM divided by the total laser intensity), $\beta$ is the FM index (defined as the amplitude of FM divided by the modulation frequency) and $\theta$ is the FM-IM phase shift.

When the three-tone beam impinges the (square law) detector, a beat note signal at the modulation frequency $\Omega$ is generated between the carrier wave and the two sidebands, which can be expressed as:

$$I \propto (E_0 + E_1 + E_{-1})^2. \tag{6}$$

The phase of the signal demodulated from the lock-in amplifier can be measured according to $\varphi = \tan^{-1}(Y/X)$. Its phase is the superposition of the optical phase of two beat note signals, and can be expressed as a function of laser tuning factor, refractive index, and absorption coefficients

Optics EXPRESS

at the three tones:

$$\varphi = \tan^{-1}\left\{\frac{\begin{array}{l}2A\beta\sin(\varphi_0-\varphi_1-\theta)-2B\beta\sin(\varphi_{-1}-\varphi_0-\theta)\\+Am\sin(\varphi_0-\varphi_1)+Bm\sin(\varphi_{-1}-\varphi_0)\end{array}}{\begin{array}{l}2A\beta\cos(\varphi_0-\varphi_1-\theta)-2B\beta\cos(\varphi_{-1}-\varphi_0-\theta)\\+Am\cos(\varphi_0-\varphi_1)+Bm\cos(\varphi_{-1}-\varphi_0)\end{array}}\right\}. \tag{7}$$

The coefficient A = exp[-$\alpha(\omega+\Omega)L$-$\alpha(\omega)L$] and B = exp[-$\alpha(\omega-\Omega)L$-$\alpha(\omega)L$]. The gas concentration can be thus determined from the phase of the beat note signal.

## 3. Experimental description

Our detection target is the characteristic absorption peak of $CH_4$ at 1653.7 nm. The experimental setup is shown in Fig. 1.

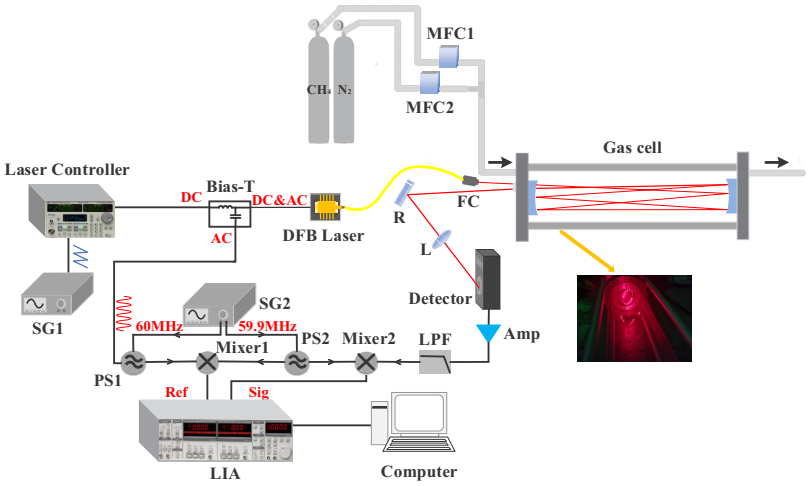


**Fig. 1.** Schematic diagram of the experimental HPSDS setup for methane detection. SG: signal generator; FC: fiber collimator; R: Reflective mirror; L: lens; Amp: amplifier; LPF: Low pass filter; PS: power splitter; LIA: lock-in amplifier; MFC: mass flow meter

The temperature and injection current of the tunable distributed feedback (DFB) laser are precisely controlled by a low-noise laser controller (LDC501, Stanford Research Systems). Due to the limited modulation bandwidth of the laser controller, a RF bias-tee circuit (ZFBT-6GW+, Mini-circuits) is used to combine a high-frequency signal and the bias current to feed into the DFB laser. The DC and AC port of the bias-tee circuit are used to access bias current and high-frequency signal, respectively. A slowly changing sawtooth signal generated by SG1 (RIGOL, DG822) is connected to the laser controller and injected into the DFB laser via the DC port of a bias-tee (ZFBT-6GW+, Minicircuits) to scan the absorption spectrum of $CH_4$. The PS1 divides the sinusoidal modulated signal with a frequency of 60 MHz from the SG2 (RIGOL, DG4162) into two channels with the same frequency and initial phase. One channel is connected to the DFB laser via the bias-tee. Hence, a three-tone beam composed of a carrier and two sidebands is generated by modulating the DFB injection current at a high-frequency sinusoidal signal. The frequency difference between the two sidebands and the carrier is 60 MHz. Another channel is connected to Mixer1 to generate the reference signal for the lock-in amplifier. The beam is coupled to a multi-pass gas cell through a fiber collimator. The effective length of the

Optics EXPRESS

cell is more than 12 meters. The output of the multi-pass gas cell is focused into a photoelectric detector (PDA10CF-EC, Thorlabs) with a lens to generate a heterodyne interference signal, which is amplified by a wide band amplifier (ZFL-500 LN+, Minicircuits) and processed with a low pass filter (SLP-150+, Minicircuits). The detected beat signal and a sinusoidal signal with slightly different frequency (59.9 MHz) generated from another channel of SG2 are mixed into the Mixer2 to obtain a beat signal with a frequency of 100kHz, which lies within the bandwidth of the lock-in amplifier (SR830, Stanford Research Systems). The dispersion phase information is obtained by extracting the first harmonic (1f) phase from the beat note signal through the lock-in amplifier.

The gas cell is filled with $CH_4$ and $N_2$, and two mass flow meters (MFC1, MFC2) control the gas flow rate. The sample with a constant flow rate is sent to the input of the gas cell, and the output is ventilated and opened. The setup ensures that all measurements are conducted with a continuous gas flow at 1atm.

The experimental setup is designed in a way that also wavelength modulated spectroscopy (WMS) may be performed on the same samples. In WMS mode, the mixer and a bias-tee circuit are removed. The sinusoidal modulation signal and the scanning sawtooth signal are superimposed on the modulation input of the laser controller, and the modulation frequency and depth are adjusted to optimize WMS performance. The output signal of the detector is directly sent to the lock-in amplifier to extract the second harmonic (2f) component for gas concentration analysis. Finally, the first harmonic phase and WMS-2f signal are recorded by a digital acquisition card (DAQ-2010, ADLink) and transmitted to the computer for data processing.

## 4. Results and discussion

IM and FM will be introduced simultaneously by directly modulating the semiconductor laser. For HPSDS, FM is unwanted, since its occurrence leads to an asymmetry in amplitude and phase of the two sidebands and, in turn, to a nonlinear relation between the peak of the output phase and the gas concentration. As suggested in Ref. [26], by carefully changing the operating point of the laser, i.e., increasing the modulation frequency and reducing the bias current of the laser, the influence of frequency modulation of DFB can be suppressed, at least to a certain extent. Based on the above principle, given the limitations of the operating bandwidth of a signal generator and detector available in our lab, in Fig. 2 we show the linear relation of the negative peak of HPSDS signals at modulation frequencies of 50 MHz, 60 MHz and 70 MHz for different $CH_4$ concentrations. In our experiments, the injection current and temperature of the laser are set to 80 mA and 28°C, respectively.

As shown in Fig. 2, in the range of 50 MHz to 70 MHz, the higher the modulation frequency, the smaller the negative peak of the HPSDS signal. It is noted that the higher modulation frequency has wider linear response curve over gas concentration. This variation relationship is critically dependent on the ratio of FM/IM sidebands determined by the tuning coefficient of the selected DFB laser, i.e., the ratio of the FM index $\beta$ to the IM index $m$. Due to the out-of-phase FM sidebands, a larger phase shift will be experienced in the center of the line. Given the frequency response characteristics of the DFB laser used ($\beta >> m$), when frequency modulation dominates, the HPSDS signal amplitude becomes much higher. So, as the modulation frequency decreases, the stronger the FM in the mixed modulation, the higher the negative peak of the HPSDS signal, and the smaller its linear range [21]. For a modulation frequency of 70 MHz, the dynamic range achieves 1400 ppm.

HPSDS has been further analyzed to assess its long-term stability and detection limit. Figure 3 shows the continuous measurements of $CH_4$ at 650 ppm for 60 minutes at three frequencies (50 MHz, 60 MHz and 70 MHz). The experimental results show that the average concentrations obtained at the three frequencies are 698.52 ppm, 635.55 ppm and 689.61 ppm, respectively. The corresponding standard deviations are 34.33 ppm, 44.91 ppm and 64.62 ppm, respectively. It

Optics EXPRESS

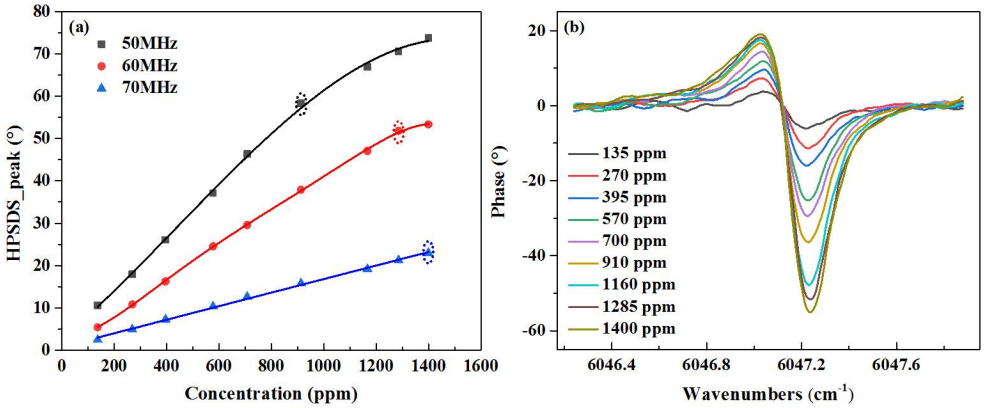


**Fig. 2.** (a) Linear relation of the negative peak of the HPSDS output phase for different modulation frequencies. (b) Measured HPSDS signals at modulation frequency of 60 MHz for different $CH_4$ concentrations.

can be seen that the 1σ precision of the system becomes worse as the modulation frequency increases, mainly because the higher the modulation frequency, the smaller the modulation depth, determined by the modulation characteristics of the semiconductor laser. In turn the received signal is more susceptible to the detector noise, limiting the detection accuracy of the system. The optimal signal averaging time and corresponding detection limit are determined by the Allan variance. In terms of sensitivity and measurement accuracy, working at 50 MHz provides better results. The detection limit of the system @50 MHz is 1.28 ppm at a longer average time of 1600 s, however, its linear dynamic range is narrow. A practical compromise, between the large linear dynamic range and the low detection limit, yielded the actual choice of 60 MHz modulation frequency used in our experiment.

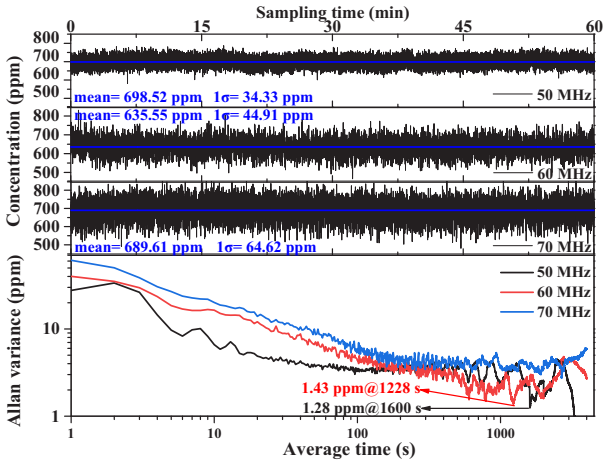


**Fig. 3.** Detection of 650 ppm $CH_4$ at three different modulation frequencies for 60 minutes together with the Allan variance diagram of the system.

In our measurements, we found that changing the frequency of the scanning sawtooth signal has a clear effect on the output phase of the HPSDS. Figure 4 shows the HPSDS signal obtained for a 400 ppm $CH_4$ sample measured at different scanning frequencies (10 Hz-40 Hz) with a modulation

Optics EXPRESS

frequency of 60 MHz, and a laser injection current of 80 mA. The simulated absorption spectra from HITRAN database in the same conditions are also shown in Fig. 4 for comparison.

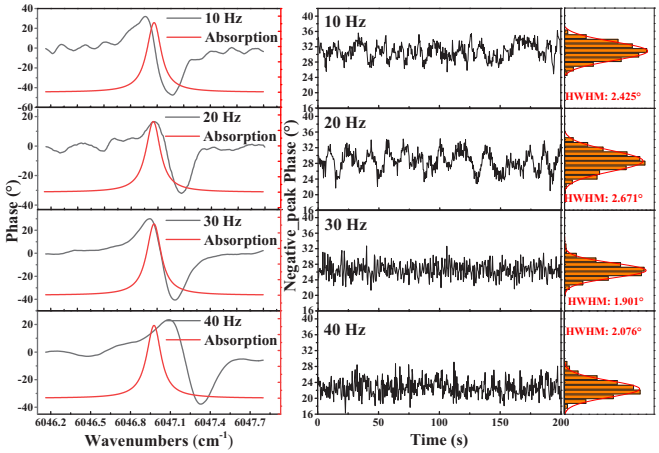


**Fig. 4.** Left panel: the HPSDS signal at different scanning frequencies (black lines) and simulated absorption spectra (red lines). Central panel: output phase fluctuations of HPSDS. Right panel: histograms of the phase distributions.

As it can be seen from the left and central panels of Fig. 4, the lower is the scanning frequency, the closer is the negative peak phase of the HPSDS result to the simulated absorption peak, whereas its signal-to-noise ratio is worse. Different scanning frequencies also affect the peak fluctuations of the output phase. In the middle and right panel of Fig. 4, the peak fluctuations of the output HPSDS phase at different scanning frequencies are compared. The fluctuations are minimized for a scanning frequency of 30 Hz, and the relative error is 7.18% for an output phase of 26.46°±1.901°. In fact, due to the limitation of the response time of the lock-in amplifier used in this study, increasing the scan frequency (improving the time resolution of the HPSDS system) corresponds to the lock-in amplifier taking many time constants to be reflected at the output, which makes the output smoother, along with lower output signal intensity. We believe that when modulating the injection current of the laser with a high-frequency signal, the injection of a low-frequency scanning signal may introduce unwanted phase fluctuations in the carrier signal. Therefore, to obtain the optimal system performance, in a trade-off between stability and complexity, we select 30 Hz as the optimal scanning frequency of the laser.

As pointed out in the previous section, the lower the bias current of the laser, the weaker the effect of FM in the mixed modulation. Therefore, the characteristics of the negative peak of HPSDS output phase are also affected by the injection current of the laser [21]. Figure 5 depicts the wavelength tuning characteristics of the 1.65μm DFB laser measured using a wavelength meter (671A, Bristol). To investigate the effect of the injection current, three sets of operating points ($I_{DC}$ = 80 mA, $T_{DFB}$ = 28 °C, $I_{DC}$ = 106 mA, $T_{DFB}$ = 25 °C, and $I_{DC}$ = 128 mA, $T_{DFB}$ = 22 °C) were chosen to tune to the target $CH_4$ absorption line and we fill the gas cell with different standard concentrations of $CH_4$ at one standard atmospheric pressure. In Fig. 6, we illustrate results about the linearity of the HPSDS signals at these three different laser settings at the modulation frequency of 60 MHz. By taking the negative peak value of 80 mA as a reference, the negative peak value of the HPSDS output phase at three injection currents is normalized to the [0,1] interval. The linear relation between the negative peak of the output phase and the gas concentration is better preserved when the bias current is closer to the threshold current of the DFB laser. The threshold current of the DFB is 10 mA.

Optics EXPRESS

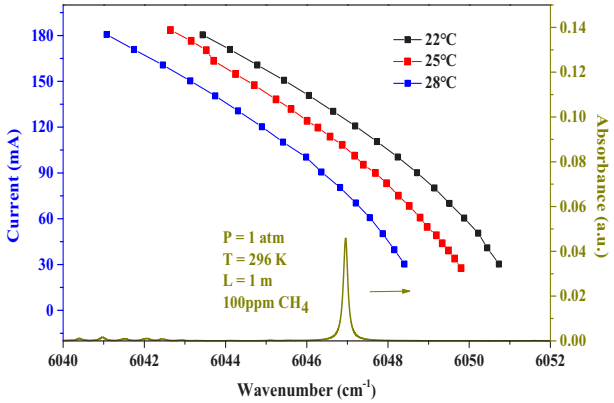


**Fig. 5.** The wavelength tuning characteristics of the 1.65μm DFB laser on the top of target absorption line of $CH_4$.

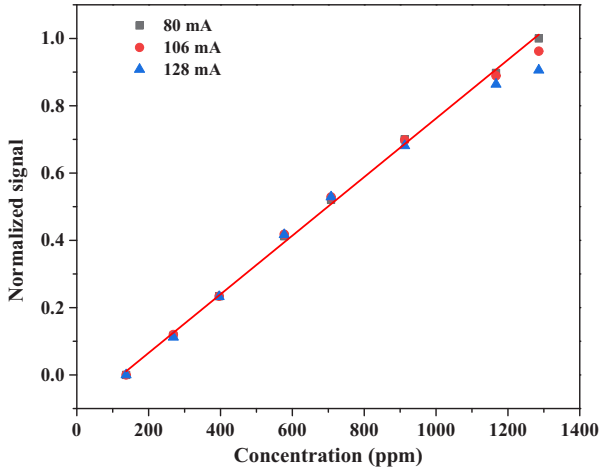


**Fig. 6.** The linear relation of the negative peak of the HPSDS output phase for different bias current of the laser. The output has been normalized.

Concerning long-term stability and detection limit performance of the HPSDS sensor at the three different bias currents (80 mA, 106 mA and 128 mA), we have measured a sample of 400 ppm $CH_4$ measured for 60 minutes. Results are shown in Fig. 7, the average detected concentrations are 367.13 ppm, 397.11 ppm and 393.81 ppm, and the corresponding standard deviations are 38.08 ppm, 39.41 ppm and 38.89 ppm, for the bias current of 80 mA, 106 mA and 128 mA, respectively. The long-term stability of the detection system is assessed in terms of the Allan variance, showing that for the bias current set to 106 mA, the detection limit of the system achieves 1.22 ppm in a longer measurement time. We thus select 106 mA as the optimal bias current of our HPSDS.

Figure 8 shows the HPSDS and WMS-2f signals measured at different $CH_4$ concentrations. For WMS-2f, the bias current of the laser is set to 106 mA, 0.14 V and 13 kHz are selected as the optimal parameters of the current WMS by adjusting the modulation depth and frequency. For HPSDS, we set the modulation frequency to 60 MHz and the bias current to 106 mA, and obtain a dynamic range of 1160 ppm, with a linear regression value $R^2$ of 0.9994. In contrast, WMS-2f shows a good linear response only in the concentration range of 135-700 ppm, with a $R^2$ value of

Optics EXPRESS

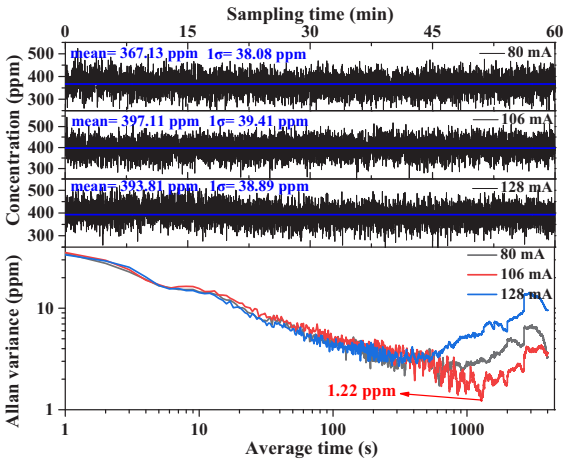


**Fig. 7.** Allan Variance Diagram of the System.

0.9976. Hence, compared with WMS, HPSDS shows a larger dynamic range, which is due to the inherent linear relation between the dispersion phase and the gas concentration.

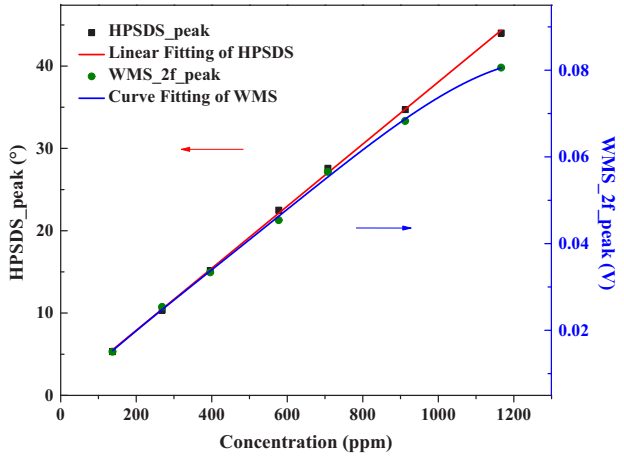


**Fig. 8.** Comparison between the linearity of HPSDS and WMS-2f at different $CH_4$ concentrations.

In order to evaluate the long-term stability of the systems, HPSDS and WMS-2f with optimal parameters are employed to measure 400 ppm $CH_4$ for 1 hour. Results, i.e. frequency histograms of the data, are shown in Fig. 9 together with the corresponding Gaussian fitting. The concentration measured by HPSDS sensor system is 397.2 ± 40.5 ppm with a relative error of 10.2%, whereas WMS leads to at measured concentration of 415.9 ± 10.8 ppm with a relative error of 2.6%. Allan variance is introduced to further analyze the long-term stability of the detection system. For HPSDS, when the integration time is 1s, the minimum detection limit of the system is 35.35 ppm, which can be improved to 1.22 ppm with an average time of 1285 s. For WMS, the minimum detection limit can reach 0.51 ppm when the integration time is 1175 s. It can be seen that the measurement precision and sensitivity of HPSDS under the current settings are not better than those of WMS, which may be due to the fluctuations of measurement phase caused by electronic cross-talk from the transceiver to the receiver [33], such as the imbalance circuit in the mixer,

Optics EXPRESS

thereby limiting the sensitivity of the system. Furthermore, the sensitivity of previous HPSDS gas sensors may be further improved by applying additional wavelength modulation to the laser to detect harmonic signals arising from phase signals [34].

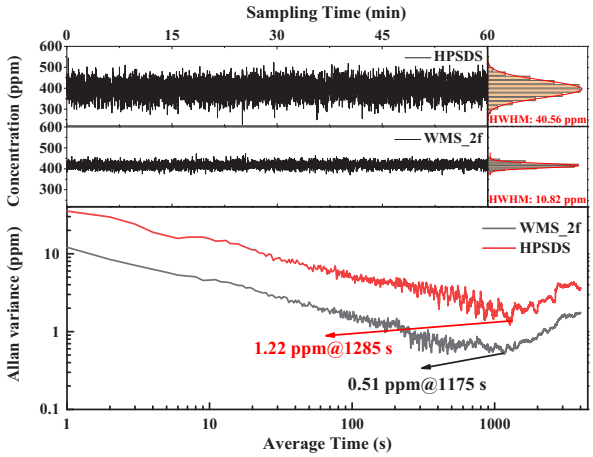


**Fig. 9.** HPSDS and WMS-2f were tested for a long time, respectively, and Allan variance is calculated to analyze their stability.

## 5. Conclusion

We have presented and implemented an HPSDS scheme where the bias current of the DFB laser is modulated directly by a bias-tee circuit to generate a three-tone laser beam. This allows us to investigate the sensing performance of HPSDS at different operating points of the DFB laser, based on the consequences of the modulation characteristics of the DFB and to demonstrating the implementation of a near-infrared HPSDS sensor for methane detection. By using the characteristic absorption peak of methane @ 1653.7 nm we have discussed in details the sensor response of the HPSDS sensing system at different modulation frequencies, scanning frequencies, and the DC bias currents of the laser. The optimal working parameters for HPSDS has been thus determined and the results are a modulation frequency of 60 MHz, a scanning frequency of 30 Hz, and a bias current of 106 mA. Our HPSDS sensor system achieves a relative error of 10.2% and a minimum detection limit of 1.22 ppm using the optimal configuration. In addition, an experimental comparison between WMS and HPSDS has been performed to compare the two techniques in terms of dynamic range, long-term stability and detection limit. Compared to the WMS, the dynamic range of the HPSDS has nearly doubled. However, long-term fluctuations in measurement data and Allan variance analysis show that the measurement accuracy and sensitivity of HPSDS are at least 2 times worse than WMS. In practical applications of gas sensing, such as gas leakage detection, it is necessary to obtain accurate concentration measurement values. Therefore, we plan to further investigate HPSDS in order to further improve its overall sensitivity and measurement accuracy.

**Funding.** The National Natural Science Foundation of China (Grant No. 42175130, 61865013, 6196501361865013); Key Research and Development Program of Jiangxi Province (20203BBG73039); National Key Research and Development Program of China (2018YFE0115700); Graduate Student Innovation Foundation of Jiangxi Province (YC2022-S746).

**Disclosures.** The authors declare no conflicts of interest.

**Data availability.** Data underlying the results presented in this paper are not publicly available at this time but may be obtained from the authors upon reasonable request.

Optics EXPRESS

## References


1. S. A. Montzka, E. J. Dlugokencky, and J. H. Butler, "Non-$CO_2$ greenhouse gases and climate change," Nature **476**(7358), 43–50 (2011).
2. C. Zhang, S. Qiao, Y. He, S. Zhou, L. Qi, and Y. Ma, "Differential quartz-enhanced photoacoustic spectroscopy," Appl. Phys. Lett. **122**(24), 241103 (2023).
3. Y. Ma, T. Liang, S. Qiao, X. Liu, and Z. Lang, "Highly sensitive and fast hydrogen detection based on light-induced thermoelastic spectroscopy," Ultrafast Science **3**, 0024 (2023).
4. X. Liu, S. Qiao, and Y. Ma, "Highly sensitive methane detection based on light-induced thermoelastic spectroscopy with a 2.33 μm diode laser and adaptive Savitzky-Golay filtering," Opt. Express **30**(2), 1304–1313 (2022).
5. Y. Li, R. Z. Wang, F. K. Tittel, and Y. F. Ma, "Sensitive methane detection based on quartz-enhanced photoacoustic spectroscopy with a high-power diode laser and wavelet filtering," Opt. Laser Eng. **132**, 106155 (2020).
6. M. Lackner, "Tunable diode laser absorption spectroscopy (TDLAS) in the process industries - A review," Rev. Chem. Eng. **23**(2), 65–147 (2007).
7. C. S. Goldenstein, I. A. Schultz, R. M. Spearrin, J. B. Jeffries, and R. K. Hanson, "Scanned-wavelength-modulation spectroscopy near 2.5 μm for $H_2O$ and temperature in a hydrocarbon-fueled scramjet combustor," Appl. Phys. B **116**(3), 717–727 (2014).
8. K. Sun, S. Wang, R. Sur, X. Chao, J. B. Jeffries, and R. K. Hanson, "Sensitive and rapid laser diagnostic for shock tube kinetics studies using cavity-enhanced absorption spectroscopy," Opt. Express **22**(8), 9291–9300 (2014).
9. J. Reid, J. Shewchun, B. K. Garside, and E. A. Ballik, "High sensitivity pollution detection employing tunable diode lasers," Appl. Opt. **17**(2), 300–307 (1978).
10. A. Behera and A. Wang, "Calibration-free wavelength modulation spectroscopy: symmetry approach and residual amplitude modulation normalization," Appl. Opt. **55**(16), 4446–4455 (2016).
11. G. B. Rieker, J. B. Jeffries, and R. K. Hanson, "Calibration-free wavelength-modulation spectroscopy for measurements of gas temperature and concentration in harsh environments," Appl. Opt. **48**(29), 5546–5560 (2009).
12. Z. Peng, Y. Ding, L. Che, X. Li, and K. Zheng, "Calibration free wavelength modulated TDLAS under high absorbance conditions," Opt. Express **19**(23), 23104–23110 (2011).
13. A. Hangauer, G. Spinner, M. Nikodem, and G. Wysocki, "Chirped laser dispersion spectroscopy using a directly modulated quantum cascade laser," Appl. Phys. Lett. **103**(19), 191107 (2013).
14. M. Nikodem and G. Wysocki, "Chirped laser dispersion spectroscopy for remote open-path trace gas sensing," Sensors **12**(12), 16466–16481 (2012).
15. M. Nikodem and G. Wysocki, "Measuring optically thick molecular samples using chirped laser dispersion spectroscopy," Opt. Lett. **38**(19), 3834–3837 (2013).
16. M. Nikodem, D. Weidmann, and G. Wysocki, "Chirped laser dispersion spectroscopy with harmonic detection of molecular spectra," Appl. Phys. B **109**(3), 477–483 (2012).
17. L. Ma, Z. Wang, K.-P. Cheong, H. Ning, and W. Ren, "Mid-infrared heterodyne phase-sensitive dispersion spectroscopy in flame measurements," Proc. Combust. Inst. **37**(2), 1329–1336 (2019).
18. G. Wysocki and D. Weidmann, "Molecular dispersion spectroscopy for chemical sensing using chirped mid- infrared quantum cascade laser," Opt. Express **18**(25), 26123–26140 (2010).
19. G. Plant, Y. Chen, and G. Wysocki, "Optical heterodyne-enhanced chirped laser dispersion spectroscopy," Opt. Lett. **42**(14), 2770–2773 (2017).
20. M. Nikodem, G. Plant, Z. Wang, P. Prucnal, and G. Wysocki, "Chirped lasers dispersion spectroscopy implemented with single- and dual-sideband electro-optical modulators," Opt. Express **21**(12), 14649–14655 (2013).
21. P. Martín-Mateos, J. Hayden, P. Acedo, and B. Lendl, "Heterodyne phase-sensitive dispersion spectroscopy in the mid-infrared with a quantum cascade laser," Anal. Chem. **89**(11), 5916–5922 (2017).
22. M. Hu, A. Ventura, J. Grigoleto, H. shi, F. Poletti, S. Yao, and W. Ren, "Trace gas detection in a hollow-core antiresonant fiber with heterodyne phase-sensitive dispersion spectroscopy," Sens. Actuators, B **363**, 131774 (2022).
23. P. Martín-Mateos and P. Acedo, "Heterodyne phase-sensitive detection for calibration-free molecular dispersion spectroscopy," Opt. Express **22**(12), 15143–15153 (2014).
24. M. Zou, L. Sun, and Li Shaomin, "Simultaneous measurement of gas absorption and path length based on the dual-sideband heterodyne phase-sensitive detection of dispersion spectroscopy," Opt. Express **29**(8), 11683–11692 (2021).
25. W. Ding, L. Sun, L. Yi, and X. Ming, "Dual-sideband heterodyne of dispersion spectroscopy based on phase-sensitive detection," Appl. Opt. **55**(31), 8698–8704 (2016).
26. A. Hangauer, G. Spinner, M. Nikodem, and G. Wysocki, "High frequency modulation capabilities and quasi single-sideband emission from a quantum cascade laser," Opt. Express **22**(19), 23439–23455 (2014).
27. Z. Wang, K.-P. Cheong, M. Li, Q. Wang, and W. Ren, "Theoretical and Experimental Study of Heterodyne Phase-Sensitive Dispersion Spectroscopy with an Injection-Current-Modulated Quantum Cascade Laser," Sensors **20**(21), 6176 (2020).
28. K. Duan, M. Hu, Y. Ji, Z. Lu, S. Yao, and W. Ren, "High-temperature ammonia detection using heterodyne phase-sensitive dispersion spectroscopy at 9.06 μm," Fuel **325**, 124852 (2022).
29. L. Ma, Z. Wang, K. P. Cheong, H. Ning, and W. Ren, "Temperature and H2O sensing in laminar premixed flames using mid-infrared heterodyne phase-sensitive dispersion spectroscopy," Appl. Phys. B **124**(6), 117 (2018).

Optics EXPRESS

30. U. Kruger and K. Kruger, "Simultaneous measurement of the linewidth, linewidth enhancement factor/spl alpha/, and FM and AM response of a semiconductor laser," J. lightwave technol. **13**(4), 592–597 (1995).
31. R. Schimpe, J. E. Bowers, and T. L. Koch, "Characterisation of frequency response of 1.5 μm InGaAsP DFB laser diode and InGaAs PIN photodiode by heterodyne measurement technique," Electron. Lett. **22**(9), 453–454 (1986).
32. J. S. Toll, "Causality and the dispersion relation: logical foundations," Phys. Rev. **104**(6), 1760–1770 (1956).
33. Jakob Hayden, Pedro Martín-Mateos, Pablo Acedo, and Bernhard Lendl, "A quantitative comparison of dispersion- and absorption- spectroscopic gas sensing," *Proc. SPIE 10110, Photonic Instrumentation Engineering IV*, 101100Z (20 February 2017).
34. M. Hu and W. Ren, "Wavelength-modulation dispersion spectroscopy of NO with heterodyne phase-sensitive detection," Opt. Lett. **47**(11), 2899–2902 (2022).